Disentangling Complex UV-Induced Relaxation Dynamics of 2'-deoxyadenosine from 30 fs to 10 ps

Vasilis Petropoulos,[a] Prachi Pandey,[b] Margherita Maiuri[a], Fabrizio Santoro,[b] Roberto Improta,[c] Giulio Cerullo*[a,d] and Dimitra Markovitsi*[e]*

[a]Dipartimento di Fisica, Politecnico di Milano, Piazza Leonardo da Vinci 32, I-20133 Milano, Italy; [b]Consiglio Nazionale delle Ricerche, Istituto di Chimica dei Composti Organo Metallici (ICCOM-CNR), I-56124 Pisa, Italy; [c]Istituto Biostrutture e Bioimmagini- Consiglio Nazionale delle Ricerche, Via De Amicis 95, I-80145 Napoli, Italy; [d]Istituto di Fotonica e Nanotecnologie-CNR, Piazza Leonardo da Vinci 32, I-20133 Milano, Italy; [e]Université Paris-Saclay, CNRS, Institut de Chimie Physique, UMR8000, 91405 Orsay, France

Corresponding authors : roberto.improta@cnr.it; giulio.cerullo@polimi.it; dimitra.markovitsi@universite-paris-saclay.fr

Supporting Information

a – Additional figures discussed in the main text

b - Tables discussed in the main text

c - Methodological Details

d - Additional computational results

a – Additional figures discussed in the main text

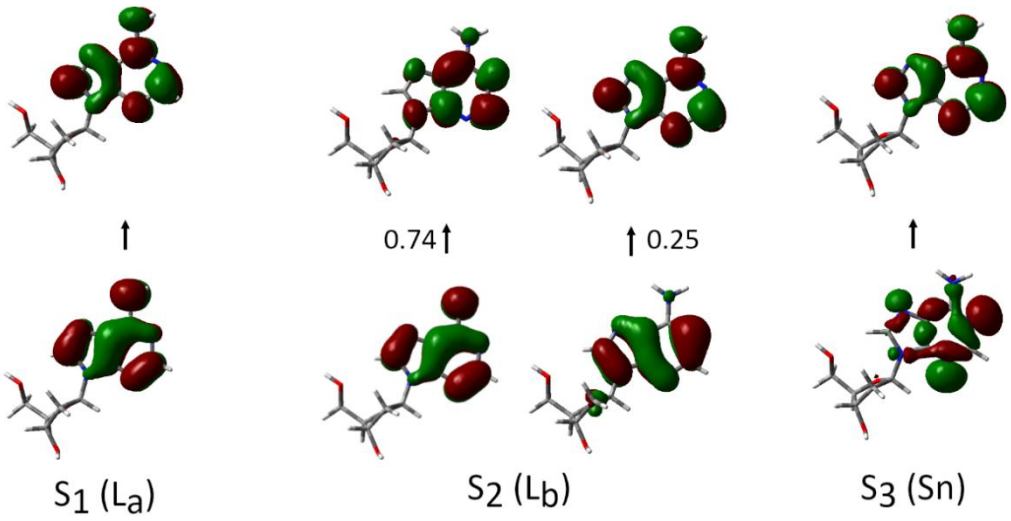

Figure S1. *Schematic description of the Natural Transition Orbitals associated to the 3 lowest energy singlet excited states of dA. PCM/TD-ω97XD/6-311+G(2d,2p) calculations. The weight of the most relevant excitations (if < 0.9) is also reported.*

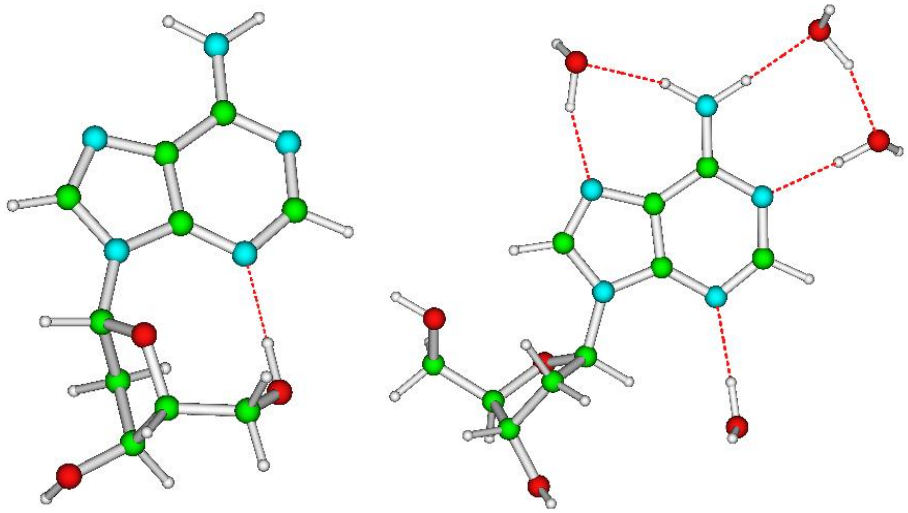

Figure S2. *Computational models adopted in this study. Left: dA; the syn conformer is depicted. Right: dA•4 H_2O; the anti conformer is depicted. In the 9-methyladenine (meA) models the sugar is mimicked by a methyl group.*

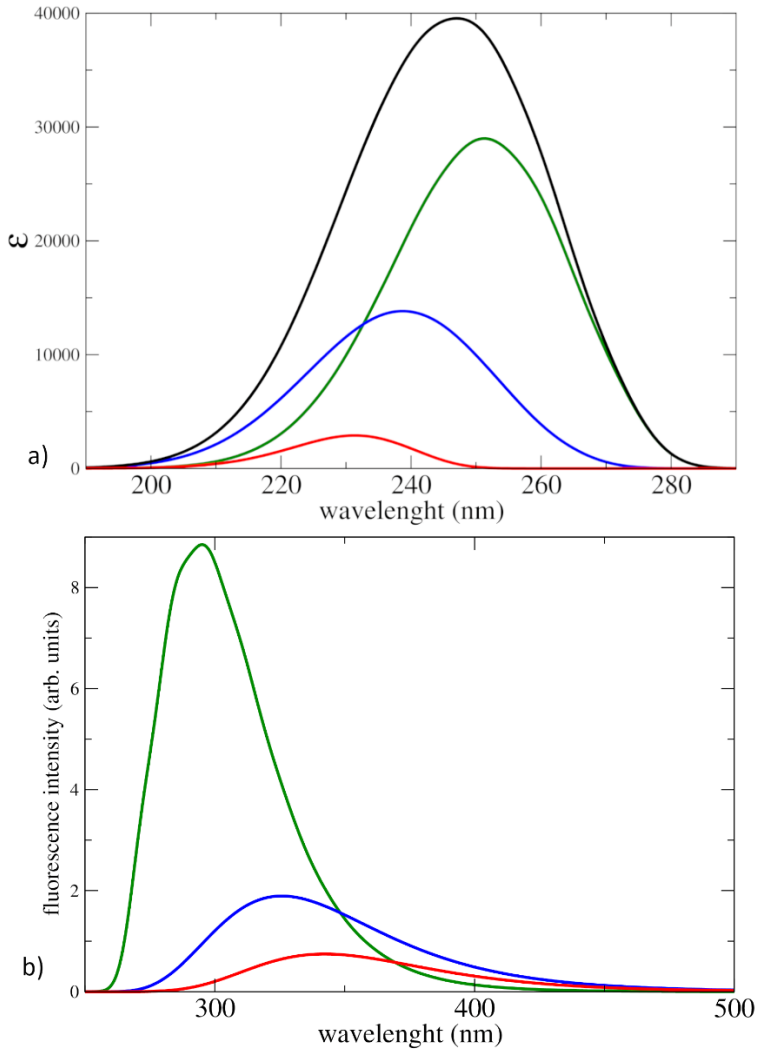

Figure S3. *Steady-state vibrationally resolved absorption (a, (molar absorptivity a, units L mol^{-1} cm^{-1})) and emission (b, arbitrary units) spectra computed for dA in water. Colour code (excitation to/emission from): Lb-min (red); L_a-min-pla (green); L_a-min-C2 (blue); sum of the spectra (black). PCM/ωB97XD/ 6-311+G(d,p) calculations. Vibrational contributions computed with the FCclasses program.*

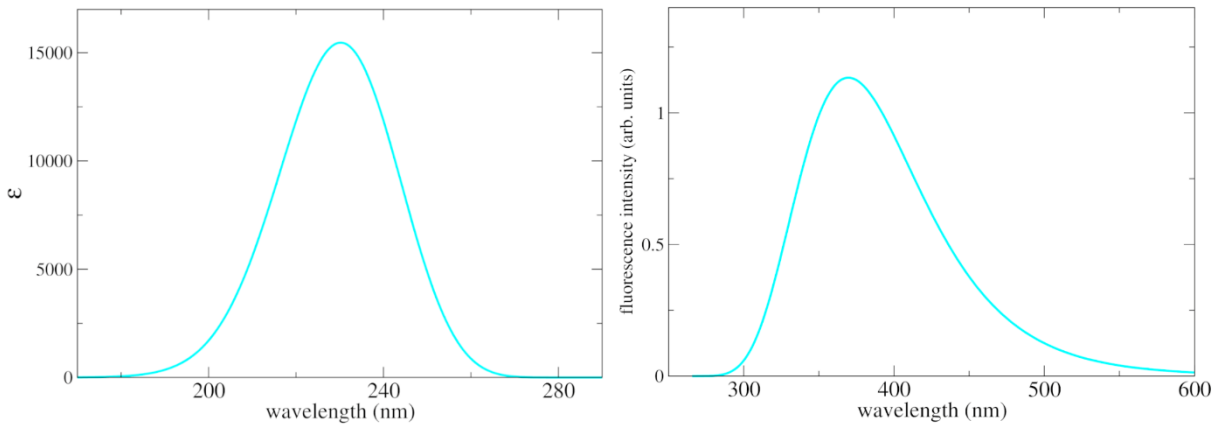

Figure S4*. Steady-state vibrationally resolved absorption (molar absorptivity, units L mol^{-1} cm^{-1}) and emission (arbitrary units) spectra computed for the La-min-C6 minimum of dA in water; PCM/TD-ωB97X-D/6-311+G(d,p) calculations. Vibrational contributions computed with the FCclasses program and the Adiabatic Hessian (AH) model.*

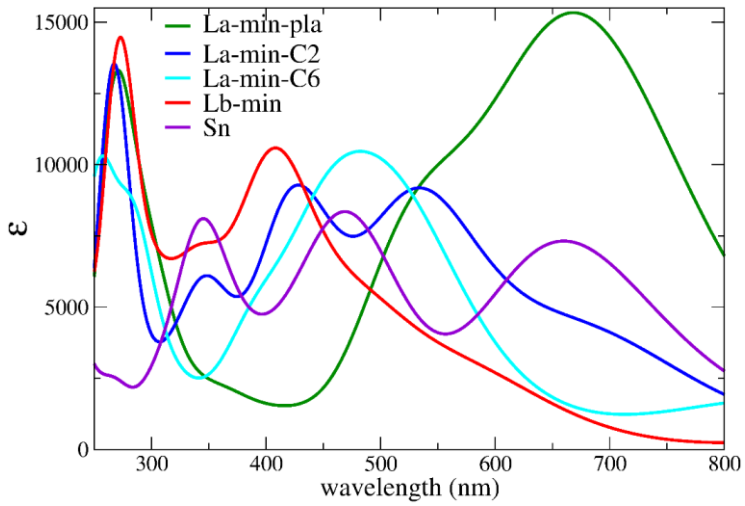

Figure S5. *ESA spectra computed at pure electronic level for the minima in the dA PES; PCM/TD-ωB97X-D/6-311+G(d,p) calculations. Each stick transition has been convoluted with a Gaussian function (HWHM = 0.25 eV) which also mimic vibrational contributions.*

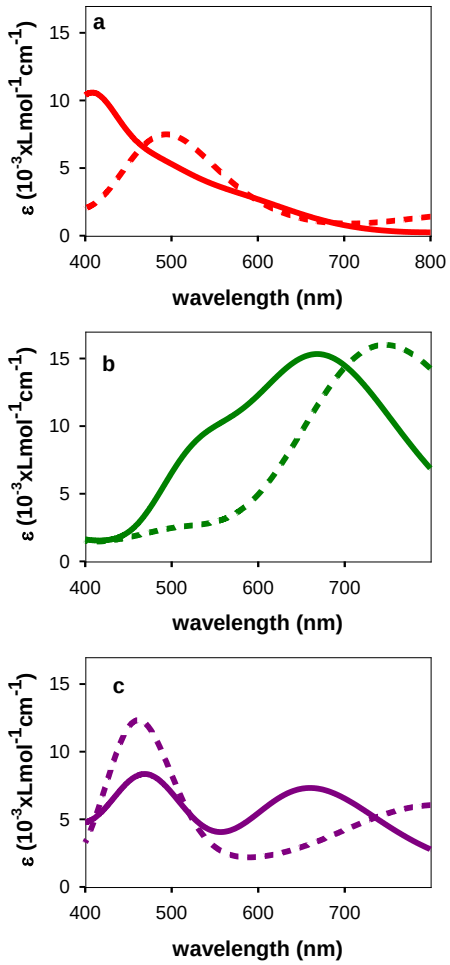

Figure S6. *Comparison of the ESA spectra computed for the three first lowest excited of dA in water, at the Franck-Condon geometry (dashed lines) and at their corresponding minima (solid lines). PCM/wB97XD/ 6-311+G(d,p) calculations. (a) L_b and L_b-min; (b) L_a and L_a-min-pla ; (c) Sn and Sn-min.*

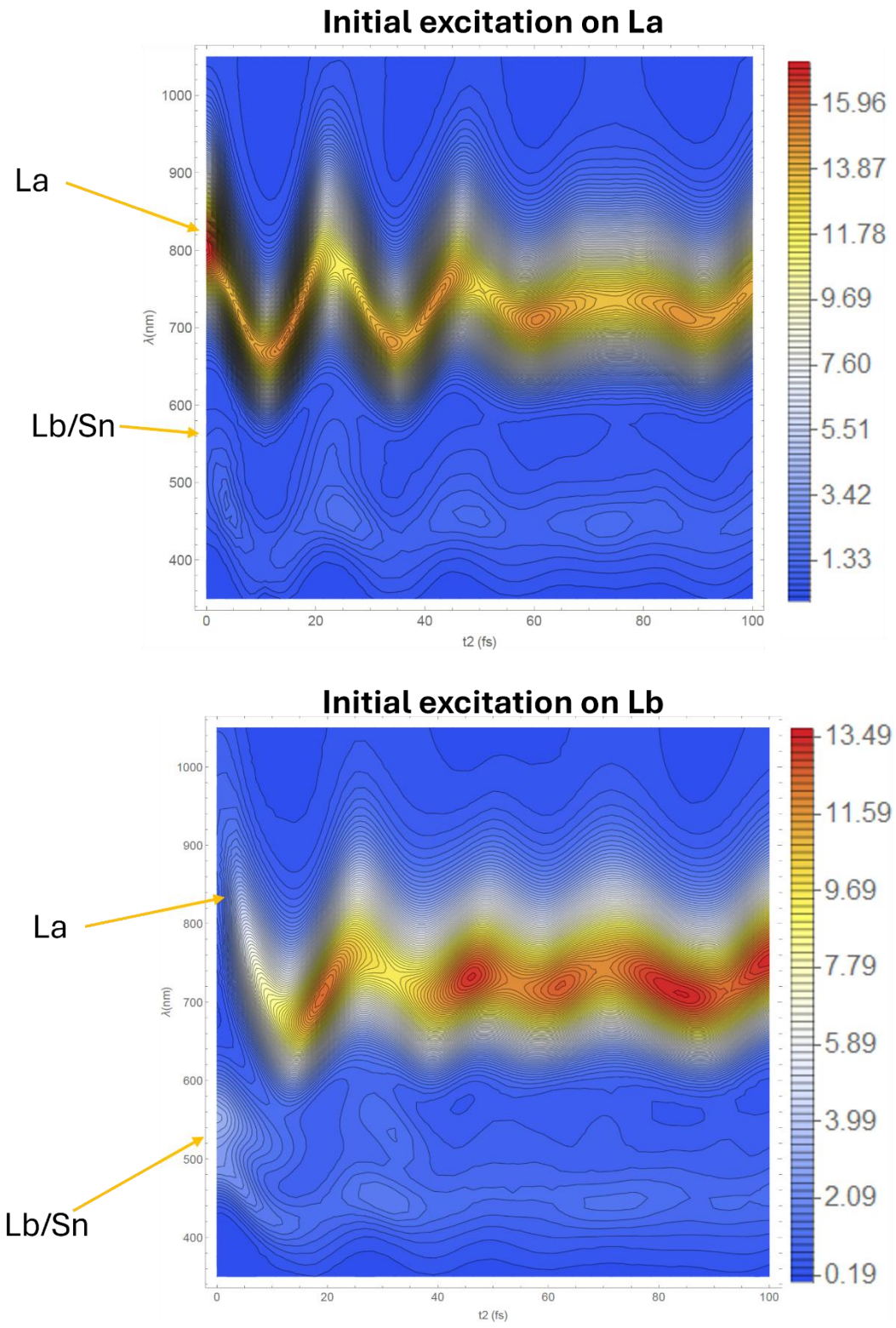

Figure S7. TA spectrum computed from nonadiabatic quantum dynamics for an initial instantaneous excitation to La (upper panel) or to Lb (lower panel)

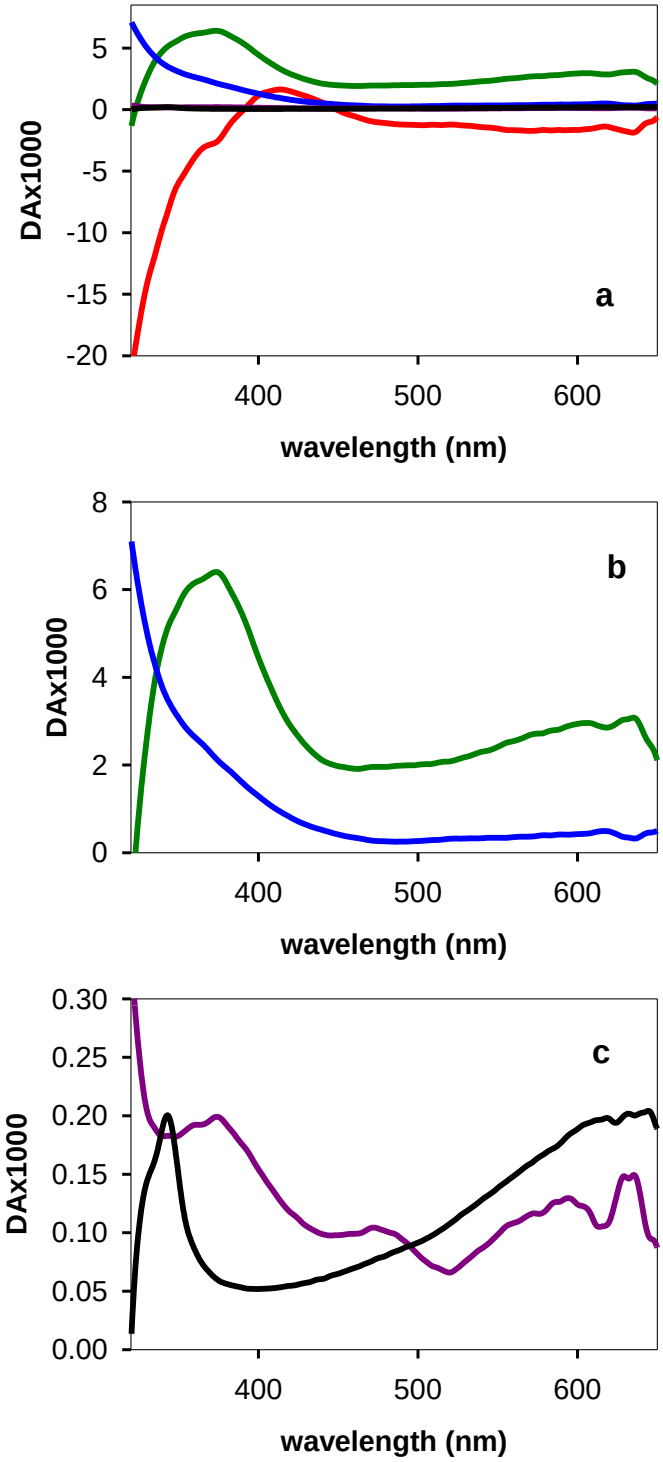

Figure S8. *Decay associated spectra retrieved from a global analysis of the TA data obtained for dA, using a 5-exponential function and including the IRF of 30 fs. The related time constants are: 55 fs (red), 150 fs (green), 410 fs (blue), 1.6 ps (violet) and long one (>> 40 ps; black);* $R^2 = 0.998$*. In order to appreciate the spectral shapes, the DAS are shown on 3 different DA scales.*

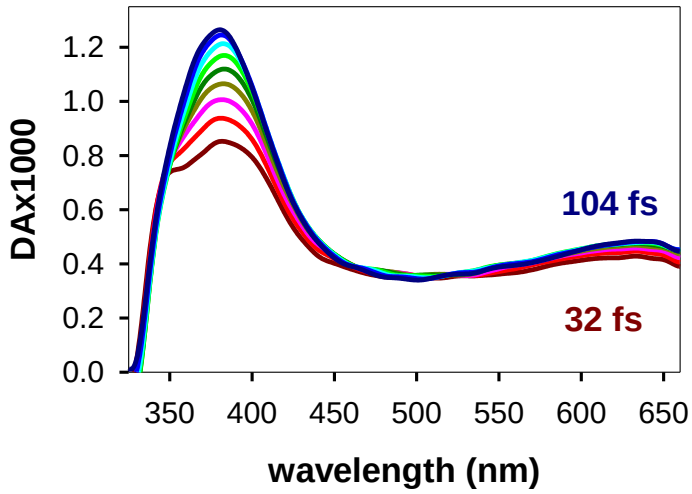

Figure S9. *TAS recorded for dA in water from 32 fs to 104 fs with 8 fs steps upon excitation at 282 nm.*
.

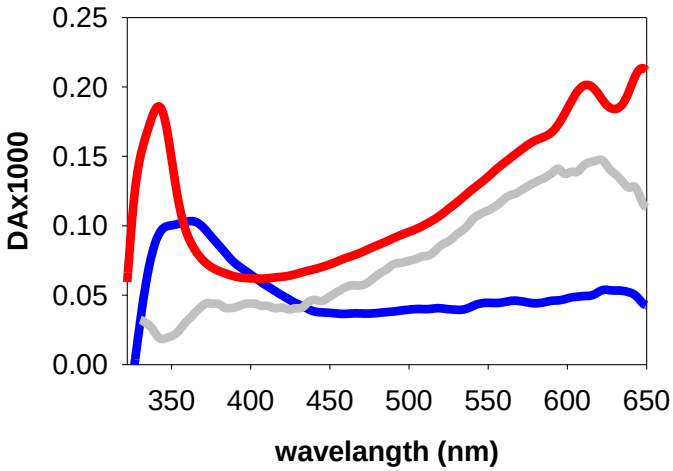

Figure S10. *TAS recorded at 10 ps for dA (red), dT (blue)*[1] *and the solvent alone (grey) under the same experimental conditions. The intensities are normalized with the energy of the exciting pulses.*

b - Tables discussed in the main text

Table S1. Vertical absorption energies (eV) and oscillator strength (in parentheses) of the three lowest energy adiabatic states of different adenosine models in water, with different solvation models. PCM/ωB97XD/6-311+G(d,p) calculations.

	meA	meA•4 H_2O	dA	dA•4 H_2O	dA *syn*
L_a	5.27(0.37)	5.22(0.40)	5.28(0.42)	5.23(0.45)	5.27(0.40)
L_b	5.42(0.02)	5.36(0.04)	5.43(0.02)	5.37(0.05)	5.42(0.03)
Sn	5.50(0.00)	5.82(0.00)	5.51(0.01)	5.83(0.00)	5.53(0.00)

Table S2. Adiabatic energies (eV) oscillator strength (in parentheses) of the three lowest energy adiabatic states of adenosine in water, in different points of their PES and different solvation models. PCM/ωB97XD/6-311+G(d,p) calculations. For each minimum the lowest energy is noted in bold and the emission energy in italics.

	L_a-min-pla	L_a-min-C2	L_a-min-C6	L_b-min	Sn-min
meA					
L_a	**4.70(0.58)** ***4.29***	**4.72(0.25)** ***3.74***	**4.70(0.26)** ***3.35***	5.81(0.34)	5.49(0.38)
L_b	5.45(0.11)	4.76(0.12)	6.04(0.10)	**4.92(0.13)** ***3.59***	6.07(0.05)
Sn	5.35(0.00)	4.56(0.09)	5.93(0.07)	6.04(0.03)	**4.79(0.04)** ***3.70***
meA•4H_2O					
L_a	**4.68(0.56)** ***4.27***	**4.73(0.32)**[a] ***3.88***	Converge to	5.70(0.43)	Converge to L_a
L_b	5.39(0.15)	5.63(0.21)	L_a-min-pla	**4.92(0.18)** ***3.84***	
Sn	5.64(0.00)	5.83(0.04)			
dA syn					
L_a	**4.71(0.57)** ***4.28***	Decay to	**4.72(0.28)** ***3.32***	5.78(0.40)	5.49(0.41)
L_b	5.48(0.12)	L_a-min-pla		**4.93(0.14)** ***3.68***	6.11(0.05)
Sn	5.38(0.01)		5.95(0.08)	6.04(0.02)	**4.83(0.04)** ***3.75***

[a] two negative frequencies (-91 cm^{-1} and -29 cm^{-1})

Table S3. Norm (eV) of the energy gradients (diagonal elements) and of the coupling vectors (off-diagonal elements) of the three diabatic states of 9methyl-adenine as predicted by the LVC model parameterized with PCM/ωB97XD/6-311+G(d,p) calculations.

	$\mathbf{L_a}$	$\mathbf{L_b}$	$\mathbf{S_n}$
$\mathbf{L_a}$	0.336		
$\mathbf{L_b}$	0.142	0.254	
$\mathbf{S_n}$	0.096	0.073	0.401

c-Methodological details

Experimental

2-Deoxyadenosine monohydrate (purity: >99%) was purchased from Sigma-Aldrich and dissolved in ultrapure water. Steady-state absorption spectra were recorded using a PerkinElmer Lambda 1050 spectrophotometer.

Transient absorption (TA) experiments were performed using an amplified Ti:sapphire laser system (800 nm central wavelength, 100 fs pulse duration, 1 kHz repetition rate).[2] A fraction of the laser output was frequency-doubled to pump a non-collinear optical parametric amplifier (NOPA), generating broadband visible pulses that were compressed with chirped dielectric mirrors and subsequently frequency-doubled in a 20-μm-thick β-barium borate (BBO) crystal to produce broadband UV pump pulses tunable across the 250–300 nm range. The UV pulses were compressed with a MgF_2 prism pair to a nearly transform-limited of 18 fs duration and characterized by two-dimensional spectral interferometry.[3] Broadband probe pulses (330–650 nm) were generated by focusing the fundamental beam into a 2-mm-thick CaF_2 plate. Pump and probe beams were non-collinearly focused onto the sample with spot sizes of 180 μm and 95 μm, respectively, and their relative polarizations set to the magic angle (54.7°). The pump pulse energy was 52 nJ.

Sample solutions (6 mL) were circulated through a quartz flow cell during the measurements, and dispersion introduced by the entrance window was pre-compensated using the prism compressor.[4] At the pump wavelength, the samples are optically thick, such that excitation is confined to the entrance region of the cell, with more than 95% of pump photons absorbed within ~0.2 mm.

The effective temporal resolution of the experiment was determined from the rise of the stimulated emission signal of the ππ* state of thymidine at 335 nm, measured under identical conditions to those used for dA, yielding an instrumental response function of 27 fs.[1] Consistent values were obtained across the probe spectrum from control nucleoside and dinucleotide measurements.[4, 5]

Computational

Ground-state geometry optimizations were performed using density functional theory (DFT). For excited-state calculations, we utilized its time-dependent extension, TD-DFT. We chose the ωB97XD hybrid functional, which includes empirical dispersion terms and long-range corrections,[6] in conjunction with the 6-311+G(d,p) basis set. All geometry optimizations were complemented by the calculation of vibrational frequencies, to ensure that the stationary points obtained correspond to true minima of the PES.

Bulk solvent effects were accounted for via the PCM model.[7] This approach occasionally complemented by the inclusion of four explicit water molecules from the first solvation shell to account for specific solute–solvent hydrogen-bonding interactions. The arrangement, illustrated in Figure S2, saturates the primary hydrogen-bond donor and acceptor sites of dA. This approach has been shown to provide a reliable description of solvent effects for other nucleobases in aqueous solution.[8]

All TD-DFT calculations were performed using the Gaussian 16 software package.[9] Vibrationally resolved spectra were computed using the FCclasses3 program.[10] The sepctra in

Figure S12 are lineshape (L) spectra.[10] Spectra were computed by using both the adiabatic Hessian (AH) and the vertical Hessian (VH) models.

ESA spectra were simulated at pure electronic level (without considering explicitly vibrational states) using equilibrium PCM/TD–ωB97XD/ 6-311+G(d,p) calculations, with the transition dipole moments between excited states determined using the Multiwfn program.[11] To generate the spectral profiles, each discrete electronic transition was broadened by a Gaussian function with a half-width at half-maximum (HWHM) of 0.25 eV which phenomenologically accounts for homogeneous and inhomogeneous broadening mechanisms.

Nonadiabatic quantum dynamical (QD) simulations were performed using the Linear Vibronic Coupling (LVC) model parameterized with TD-DFT computations on the grounds of a maximum-overlap diabatization technique as implemented in the freely available code Overdia 1.0,[12, 13] considering the three lowest adiabatic states at the Cs ground state geometry as reference to define L_a, L_b and S_n diabatic states. Vertical energies, energies of the LVC diabatic states at the LVC minima of each of them, and the modules of the gradient λ_{ii} and inter-state coupling vectors λ_{ij} with i $i \neq j$ are given in Tables S3-S6.

Wavepacket propagations were performed with the multilayer (ML) version of the multiconfigurational time-dependent Hartree (ML-MCTDH) approach,[14-18] as implemented in the Quantics code. For the primitive basis set, we adopted Hermite discrete variable representation (DVR), as appropriate for harmonic potentials, and we solved the ML-MCTDH equations of motion using a variable mean field (VMF) propagator with a 5th order Runge-Kutta integrator with a step of size 10^{-7}.[19] Further details on the expression of the wavefunction are given through the ML tree in Figure S11, where the normal modes are indicated as "v*n*" where "n" is an integer label in order of increasing frequency.

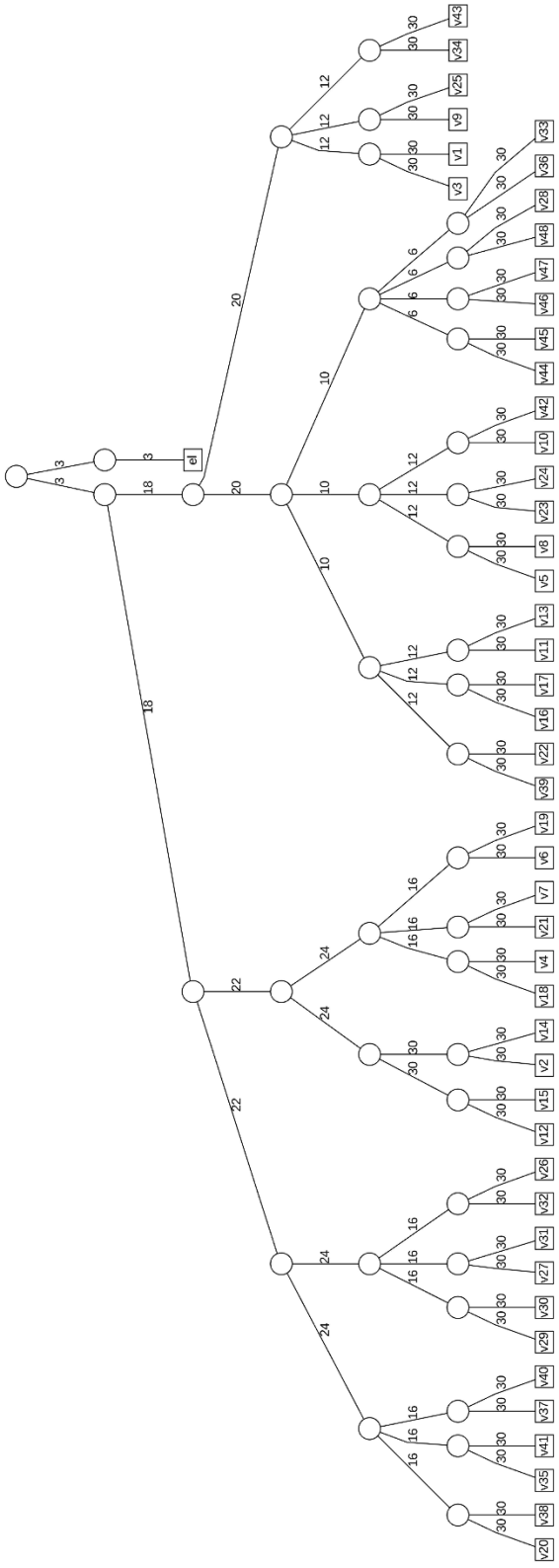

Figure S11 *Schematic tree representation of the ML-MCTDH wavefunction. From the right, the rectangular boxes represent the vibrational modes labelled in order of increasing frequency whereas the number of DVR points is reported on the lines departing from the rectangles. From the left, the circles represent the different layers of the function whereas the numbers along the connecting lines just to the right give the corresponding single particle functions*

Time-resolved pump-probe spectra were computed from the QD simulations applying the approximate short-time expression derived in Ref [20],

$$S(t_2,\omega) = \sum_{ef} \left|\mu_{ef}\right|^2 \rho_{ee}(t_2) \frac{e^{-\left(\omega-\omega_{ef}(t_2)\right)^2/2\xi_{ef}^2(t_2)}}{\xi_{ef}(t_2)\sqrt{2\pi}} \quad \text{(S1)}$$

where "e" are the coupled states excited by the pump (in our model L_a, L_b and S_n), "f" are the final states (listed in Table S6) reached after absorption of the probe from the "e" states, $\left|\mu_{ef}\right|$ is the module of the corresponding electric transition dipole, $\rho_{ee}(t_2)$ is the population of state "e" at time t_2 after the pump, $\omega_{ef}(t_2)$ and $\xi_{ef}(t_2)$ are respectively the energy gap and its corresponding standard deviation between states "e" and "f" integrated over the wavepacket running on state "e" at time t_2.

Whereas time -resolved spectra has been reported multiple times, the approach we follow here encodes some novelty. In many contributions in literature, time resolved spectra are computed in a classical approximation, i.e. repeating simple electronic computation at molecular structures extracted at different times during a trajectory surface hopping computation, and obtaining the spectra from the distribution of transition energies and dipole strengths, usually applying a Gaussian phenomenological broadening.[21] In other cases, a number of approximations are adopted to simplify the full quantum expression.[22] The most commonly approximations ones are (i) the approximation of the electronic populations in terms of a kinetic model (master equation); the (ii) the simplification of the computation of the overlaps between the wavepackets running on the different PES with the analytical models like the second-order cumulant expansion of Gaussian fluctuations.[23, 24] The latter simplification is valid in the limit of displaced oscillator models and invokes the absence of transport (change of populations due

to nonadiabatic transitions) at the times for which such overlaps are computed (i.e. the time interval Fourier-transformed to obtain the signal).

Starting from a fully quantum dynamical expression of the pump-probe spectra in the limit of impulsive pump and probes, recently some of us re-derived this hierarchy of approximations and compared their different predictions for a LVC model of pyrene.[22] In that contribution it was showed that the full quantum dynamical computation is doable thanks to MCTDH approach, but it is rather cumbersome. In a following paper in 2024,[20] the same authors introduced a simplified version which compute the time-dependent vibronic wavepackets overlap in a short time approximation. This latter approximation, give rise to the expression in Eq. S1 that is used in the present contribution. For LVC models this approach is extremely convenient from the computational point of view, requiring a negligible additional cost with respect to the standard QD simulation of the coupled states. These advantages make the computation easily at hand also for ML-MCTDH propagations considering all the nuclear coordinates (48 in 9meA). It fully describes the effect of the time evolution of the quantum electronic populations and provides transient spectra whose central position and width $\omega_{ef}(t_2)$ and $\xi_{ef}(t_2)$ are computed at a quantum dynamical level after the propagation through suitable expectation values.[20]

The main limitation of Eq S1, with respect to the fully quantum expression, is that this approach washes out the vibronic resolution of the transient spectra. However, in these systems such vibronic structure would be dominated by features mostly related to high-frequency collective stretching modes, which could be appreciated only with measurements with a sub 10 fs resolution.

d-Additional computational results

The vibrational contribution to the absorption spectra can be included by using different approaches,[25] the two most-used ones being the adiabatic Hessian (AH) and vertical Hessian (VH) models. In the former, the full vibrational analysis is performed on the minima of the ground of the excited states. In the latter, the Hessian of all states is computed at the equilibrium geometry of the ground electronic state. When the minimum of the excited state provides significant distortion along several large-amplitude vibrational modes with respect to the ground-state minimum (as it happens for the non-planar L_b-minimum), the VH model affords a more solid estimate of vibrational effects on the absorption spectrum. We have thus computed the absorption spectrum of dA using both the AH and VH approaches (see Figure S8). Interestingly, at the VH level, the maxima associated with the L_a and L_b absorption spectra are very close in energy.

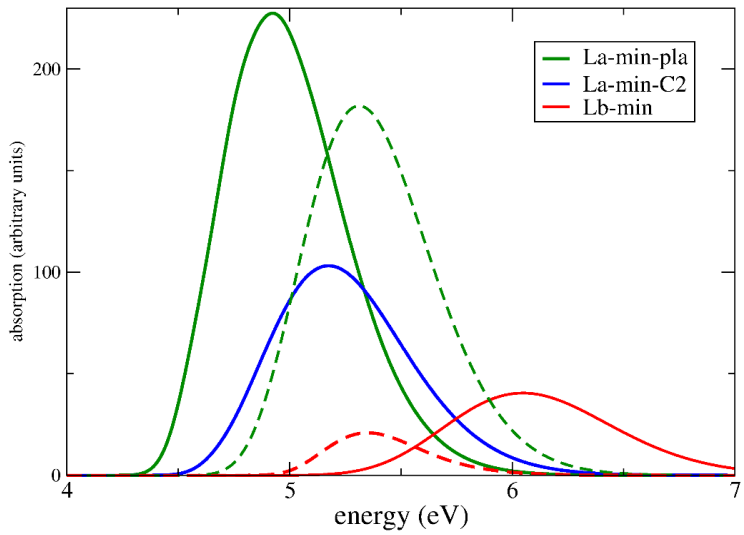

Figure S12 *Lineshape absorption spectrum computed for dA in water; PCM/TD-ωB97X-D/6-311+G(d,p) calculations. Vibronic effects included with the FCClasses program, using the Adiabatic Hessian (continuous lines) or the Vertical Hessian (dashed lines) approaches.*

Additional ESA spectra

In order to check the reliability of the adopted computational method, we computed the ESA spectra for the FC point of the 9H-adenine tautomer in the gas phase, at the TD-ωB97X-D/6-

311+G(d,p) level and compared our results with the literature data obtained with other ab initio methods.[26] Our spectra (Figure S9) are in good agreement with those provided by EOM-CC3 (available only below 2 eV) and EOM-CCSD calculations (Figure 7 in reference [26]). Moreover, in the investigate energy range, the ESA spectra of L_a and L_b are also similar to that obtained at the RASPT2 level [27](see Figure 4 in the SI of ref. 20).

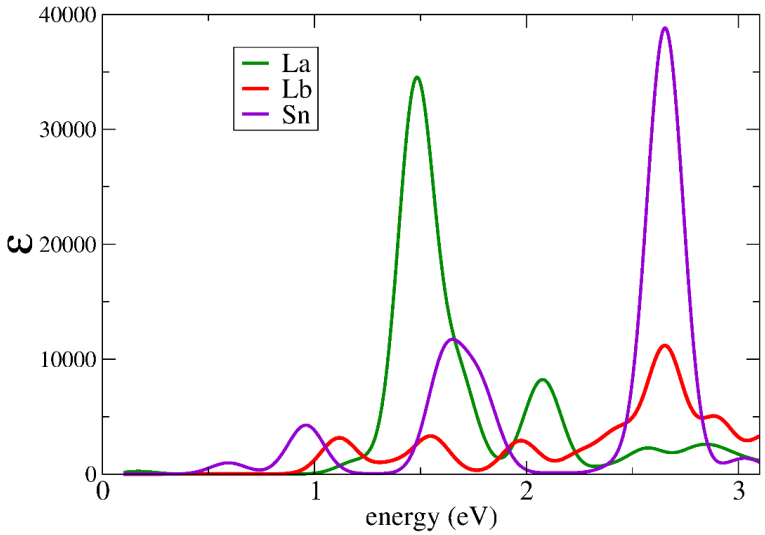

Figure S13. *ESA spectra computed for the FC point for ade-9(H) in the gas phase; TD-ωB97X-D/6-311+G(d,p) calculations. Each stick transition has been convoluted with a Gaussian function (HWHM = 0.1 eV).*

For L_a, CC3 predicts peaking at ~1.4 eV and, a shoulder at 1.7 eV and a tail in the red, in very good agreement with the TD-ωB97X-D/6-311+G(d,p) level, where the two bands are slightly closer and the higher energy one is, therefore, less visible. The two bands are present also in the CCSD spectrum, but their relative intensity is reverted with respect to the predictions of CC3 and TD-ωB97X-D.[26] A fairly intense absorption (though weaker, than the features below 2 eV) is predicted in the 2-3 eV energy range. This broad band is also present in the ωB97X-D/6-311+G(d,p) spectrum, but its intensity is underestimated with respect to the CCSD predictions.

For L_b, both CC3 and CCSD predict the presence of slightly above 1 eV and at 1.6 eV, and, according to CCSD, the most intense absorption band falls around 2.7 eV. This is the same picture provided by TD-ωB97X-D calculations (Figure S9).

Finally, for Sn, CC3, CCSD and ωB97X-D provide qualitatively similar spectra: a first band at ~1 eV, a broad band at ~1.8 eV (resulting from several peaks) and a peak at 2.5 eV. On the other hand, the relative intensity of the different ωB97X-D peaks is quite different with respect to those predicted by CC3 and CCSD, with the relative intensity of the 1.8 eV and 2.5 eV bands being reverted.

In Figures S10, S11, and S12 we report the ESA spectra computed for all the minima (Table S1 and S2) including La-min-C6 of dA for different solvation models (i.e. including or not the first solvation sphere) and for the *syn* tautomer. The results discussed for dA in the main text are fully confirmed.

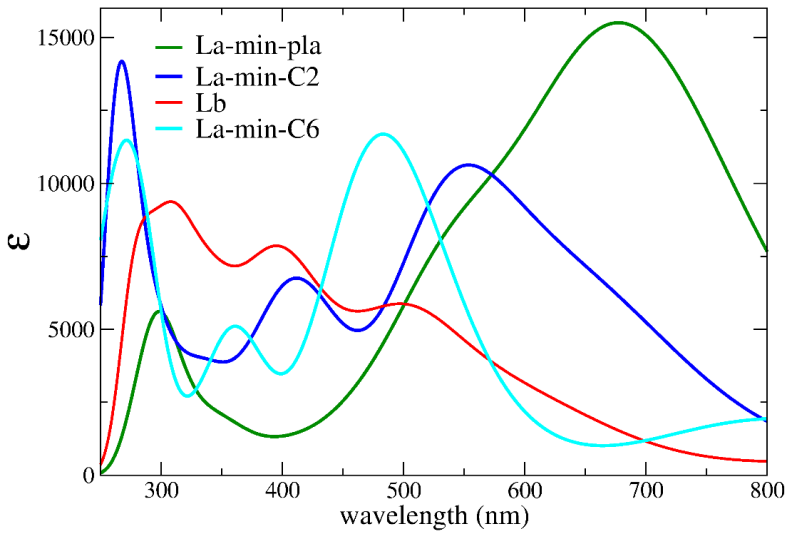

Figure S14. *ESA spectra computed for dA•4 H_2O; PCM/TD-ωB97X-D/6-311+G(d,p) calculations. Each stick transition has been convoluted with a Gaussian function (HWHM = 0.25 eV).*

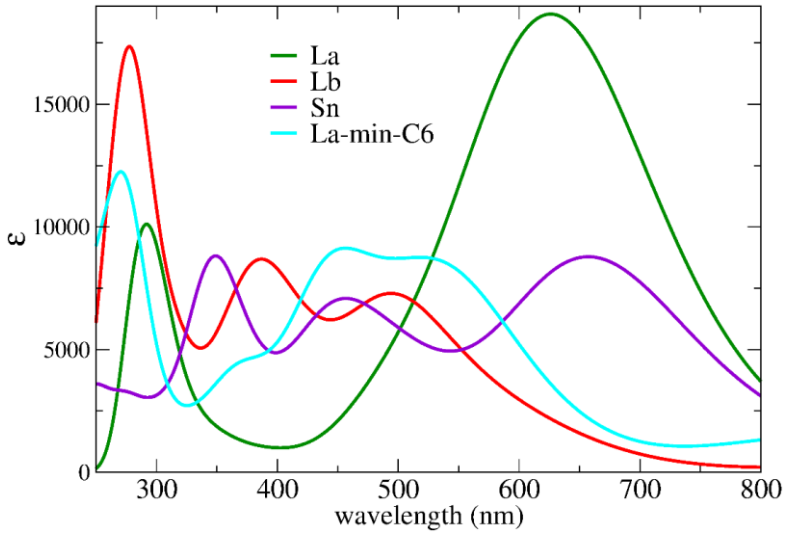

***Figure S15**. ESA spectra computed for dA syn conformer. All the spectra have been computed at PCM/TD-ωB97X-D/6-311+G(d,p) level. Each stick transition has been convoluted with a Gaussian function (HWHM = 0.25 eV).*

As anticipated in the main text, the spectra of La-min-C6, exhibit a strong maximum at 500 nm. Based on the comparison with the experiments, where this feature is never present, we can conclude that this minimum does not play a significant role in the photoactivated dynamics.

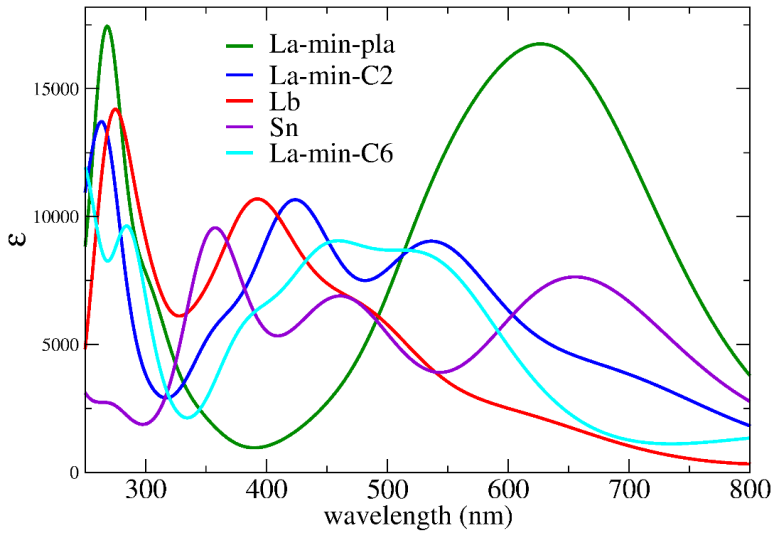

***Figure S16**. ESA spectra computed for meA; PCM/TD-ωB97X-D/6-311+G(d,p) calculations. Each stick transition has been convoluted with a Gaussian function (HWHM = 0.25 eV).*

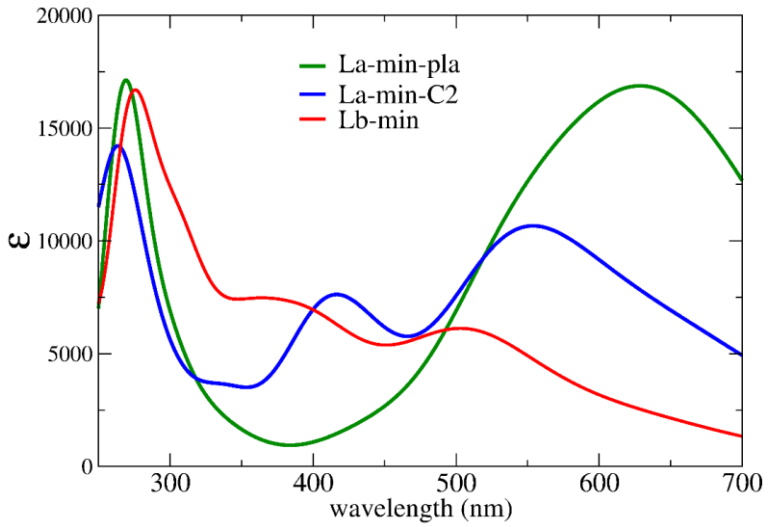

***Figure S17**. ESA spectra computed for meA•4 H_2O; PCM/TD-ωB97X-D/6-311+G(d,p) calculations. Each stick transition has been convoluted with a Gaussian function (HWHM = 0.25 eV)*

In Figures S13 and S14 we report the ESA spectra computed for the different minima located in the meA model (where the sugar is mimicked by a methyl group). The spectra are very similar to those predicted for dA, indicating that the sugar has a modest effect on the ESA and supporting the robustness of our conclusion.

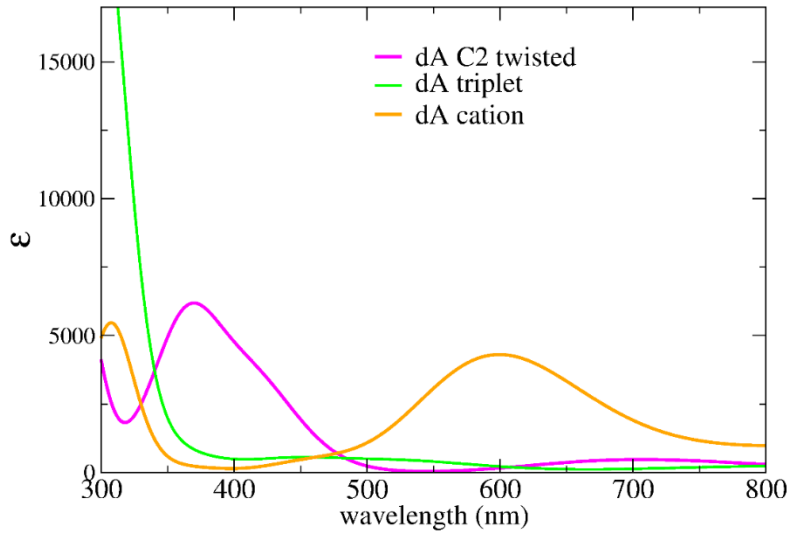

***Figure S18**. ESA spectra computed for other relevant structures of dA; PCM/TD-ωB97X-D/6-311+G(d,p) calculations. Each stick transition has been convoluted with a Gaussian function (HWHM = 0.25 eV)*

In Figure S15 we report the absorption spectra predicted for three additional potentially relevant species, i.e. the lowest energy triplet minimum of dA, the dA radical cation and the

twisted excited-state minimum located in the proximity of the crossing region with the ground electronic state (see also next subsection).

LVC Hamiltonian and Direct simulation of the spectra from QD

In Table S4, we report the vertical excitation energies computed for the planar S_0 minimum of meA, including or not four water molecules of the first solvation shell. As explained in the main text, the stability of S_n should indeed be intermediate between that obtained including only bulk solvent effects with PCM and that predicted when the first solvation shell is included in the calculations. Therefore, in the last line of the Table we also report the values obtained by averaging the energy gaps with these two different models. In Table S3 and S5-S6, we report further information for the LVC Hamiltonian obtained for the three diabatic states L_a, L_b, and Sn. The absolute stability of the minima predicted by the LVC model (Table S5), with respect to the corresponding planar minima obtained with true TD-DFT geometry optimizations (Table S2) is underestimated, as the former are constrained to be planar (as the S_0 minimum) and are obtained with an harmonic extrapolation from the FC point.

Table S4 Vertical excitation energies (eV) of the first three excited states of meA computed with PCM and with PCM on a cluster with 4 H-bonded water molecules. Last line "average" reports the average of the data in the two first lines. wB97XD/6-311+G(d,p) calculations.

at S_0 geometry	**L_a**	**L_b**	**S_n**
PCM	5.271	5.425	5.501
PCM+4H_20	5.222	5.364	5.822
average	5.247	5.395	5.662

Table S5. Energies (eV) of the first three excited states of 9meA computed in the S_0 minimum and in the minima of the three diabatic states obtained with harmonic approximation within the LVC model. All minima are computed in Cs symmetry. Top lines report the results of the LVC parameterized with PCM model (PCM) and bottom lines the results of the LVC model obtained by the previous one simply vertically shifting the harmonic potential energies of the three states so to have the "average" vertical excitation energies reported in Table S1. Energies are reported

with respect to the energy of S0 in its minimum. The energy of each state in its own minimum is reported with bold characters.

	L_a	**L_b**	**S_n**
geometry	**PCM**		
S0-min	5.271	5.425	5.501
L_a-min	**4.951**	5.455	5.428
L_b-min	5.188	**5.219**	5.624
S_n min	5.427	5.891	**4.952**
	average model		
S_0 -min	5.247	5.395	5.662
L_a-min	**4.927**	5.425	5.589
L_b-min	5.164	**5.189**	5.585
S_n-min	5.403	5.861	**5.113**

The comparison between the values in Table S5 and Table S2 (4.70, 4.92, 4.79) shows that the amount of this destabilization is 0.25 eV for La-min, 0.32 eV for L_b-min, and only 0.16 eV for Sn-min. Moreover, whereas in L_b-min (strongly non-planar) L_b is the lowest energy excited state, and it is significantly more stable than L_a, even in the LVC L_b minimum L_a is slightly more stable than L_b. As a consequence, as anticipated in the main text, our QD simulations, being based on this LVC Hamiltonian, are expected to underestimate the population of L_b, whereas that of Sn could be overestimated. In particular, in the 'real' system a part of the L_b population, created by direct excitation or due to the vibronic coupling with L_a, could be transiently trapped in the L_b-min, where L_b is much more stable than the other states. On the contrary, in our LVC model the decay to the most stable L_a-min-pla is very fast and effective. The data in Table S3 show that the three states are all remarkably coupled, with the largest coupling being between L_a and L_b states.

The time evolution of the electronic diabatic populations L_a, L_b and S_n, starting from an initial excitation on either L_a or L_b was computed by a ML-MCTDH propagation including all the 48 normal coordinates of meA and reported in Figure 3 of the main text.

By definition, diabatic states do not depend on the nuclear coordinates and therefore retain their electronic character during the dynamics. In our model, their mixing give rise to the three lowest excited adiabatic states S_1, S_2 and S_3 ordered in term of energy, which are obtained by the diagonalization of the potential energy surface matrix at each point of the coordinate space. Therefore the composition of the adiabatic states in term of diabatic states change with the nuclear coordinates.

Considering a specific molecular structure (a point in the coordinate space), in Cs symmetry (i.e when the ring is planar), S_n (A'' irreps) is decoupled from L_a and L_b (A' irreps) by symmetry, whereas L_a and L_b can mix. However, inspection of the TD-DFT coefficients and of the molecular orbitals allowed us to qualitatively assign a clear diabatic character (L_a, L_b or S_n) to at all the relevant molecular structures discussed in the text.

The situation becomes more complex when we abandon a classical pointwise description of the electronic states and we do consider the existence of the nuclear wavepacket. In that case the adiabatic populations S_1, S_2 and S_3 need to be computed through an integration in all coordinates of the coordinate-dependent diabatic-to-adiabatic transformation, a procedure that becomes more and more cumbersome and prone to errors at the increase of the number of coordinates. This transformation, which has been sometimes be reported in literature for smaller models up to 10 nuclear coordinates,[28] came out to be out of reach for our QD simulations including all 48 coordinates. Therefore, we produced a number of reduced dimensionality models, and propagated the nuclear wavefunction with MCDTH (single set formulation) trying to balance accuracy and computational feasibility.

Figure S19 show that a model including the 10 most important modes (7 belonging to A' irreps and 3 belonging to A'' irreps) captures semi-quantitatively the time evolution of the diabatic populations. The only discrepancies are some fast but small-amplitude oscillations in the dynamics starting from L_a, quenched by the additional 38 modes, and some significant oscillations of the L_a and L_b populations for a dynamics initiated on L_b, which are again quenched by the additional 38 modes, making the two populations converge faster to pseudo-stationary values (~0.85 for L_a and ~0.10 for L_b, respectively).

The computation of the adiabatic populations for this reduced dimensionality model is doable with the ***adpop*** utility of Quantics, although it requires the necessity to employ the tight option and the sum of the adiabatic populations does not sum exactly to 1. Analysis of the adiabatic populations reported in the bottom panels of Figure S19 interestingly indicate that, even a time zero, an excitation of L_a or L_b diabatic states actually translate into the population of both S_1 and S_2 states (respectively by ~70% and ~20% for L_a and ~25% and ~65% for L_b), and some small population of S_3 too. At later times, either starting from L_a or L_b most of the population transfer quickly to the lowest adiabatic states S_1. The similarity between S_1 and L_a populations indicate that the wavepacket mainly visits region of the coordinate space where S_1 has a predominant L_a character.

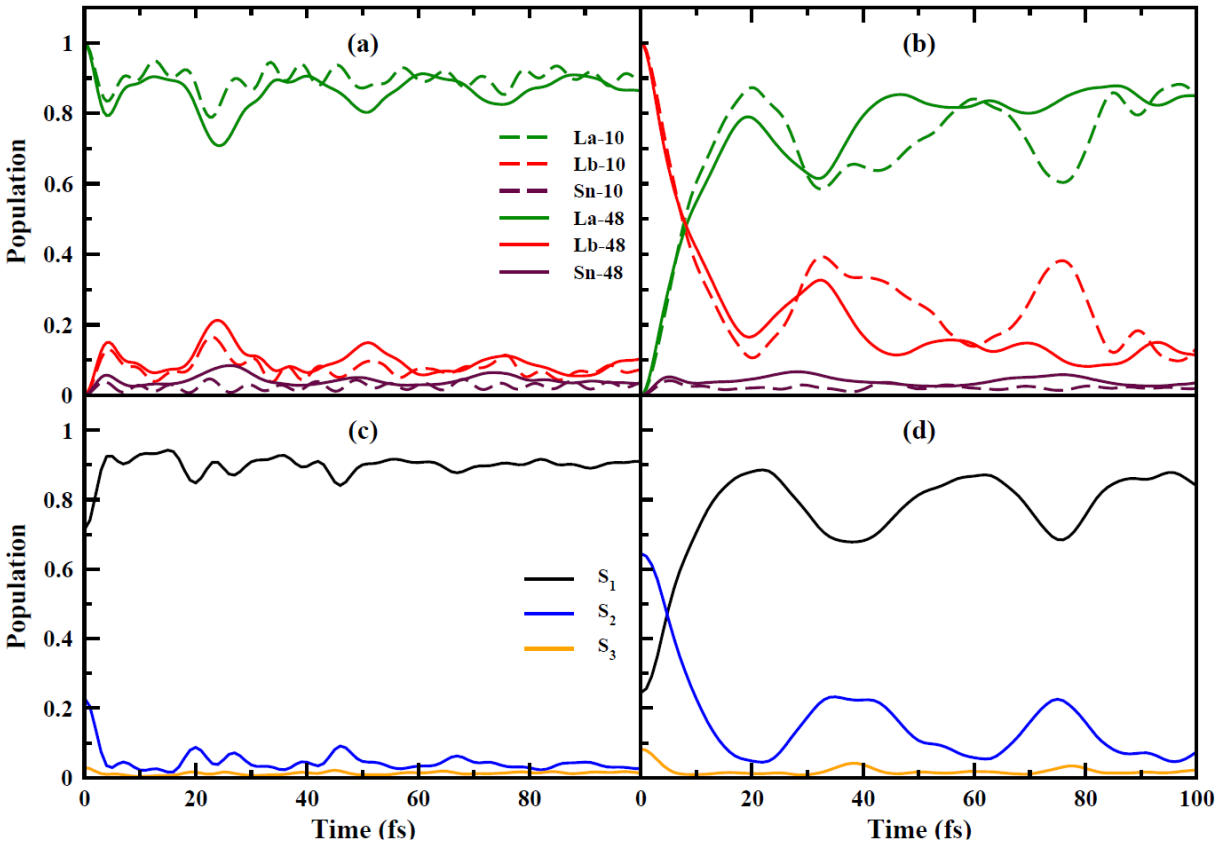

Figure S19 *Time evolution after an initial excitation* L_a (left) or L_b (right.) *Top panel compare the diabatic populations predicted by ML-MCTDH propagations using all 48 normal coordinates ("-48" labels) and by MCTDH (single set) on the grounds of a reduced dimensionality model including the 10 most important coordinates, 7 A' and 3 A'', ("-10" labels). Bottom panels report the corresponding adiabatic populations S1, S2 and S3 computed for the reduced model with 10 normal coordinates.*

As a next step, on the grounds of the ML-MCTDH simulations including all the 48 nuclear coordinates, we have simulated the time-resolved (TR) ESA spectra of meA in water, by using the procedure described in the Computational Details section above, and considering for each of the three diabatic states, the higher excited states with the largest transition dipole moments, as detailed in Table S6. The TR spectra obtained following excitation of L_a or L_b are reported in the top and bottom panels of Figure S7, respectively.

Table S6. Energies of the high-lying states most strongly coupled to the La Lb and Sn states of meA by dipole transitions and corresponding dipole strengths. All computations in PCM at the equilibrium geometry of the ground state

	VEE(eV)	**Dipole strength (au)**		
		L_a	L_b	S_n
S7	6.583	0.00	0.00	1.55
S9	6.956	5.40	0.49	0.00
S11	7.163	0.00	0.00	1.55
S14	7.416	0.00	0.00	1.34
S19	7.781	0.43	1.09	0.00
S22	8.108	0.13	0.80	0.00
S26	8.288	0.00	0.00	3.59

The two spectra are qualitatively very similar. As shown in Figure 3 of the main text, the strong vibronic coupling between L_a and L_b (Table S5) leads to a significant (15~20%), and ultrafast, population of this latter state also following excitation of La. On the other hand, the large majority of the population excited on L_b decays to L_a. As a consequence, in both panels, we observe a very strong peak on the red, associated to L_a, shifting from 800 to 680 nm in the first 10 fs and reaching an almost constant value of 700 nm in 50 fs. Simultaneously, a less intense peak, mainly associated to L_b ESA, appears below 600 nm, and shifts to 450 nm already in 20-30 fs. The computed TA spectra are qualitatively consistent with the experimental ones in the 0-100 fs time scale, and the quantitative discrepancies are explained by the limitations of our computational model, which we have discussed above.

The initial blue-shifts found in both peaks are associated to the motion of the WP from the FC region to the (planar) minima of L_a and L_b, as evidenced also in the 'static' ESA in Figure S6.

The predicted ultrafast oscillations of the signals (Figure S7) with the period of the fastest molecular vibrations cannot be observed in experiment with the achievable time resolution. On the other hand, the peaks are slightly red-shifted with respect to the experimental ones. This is due to the underestimation of the stability of the LVC minima compared to the 'real' ones, leading to a decrease of the energy gap between L_a and L_b on one side and on the other side the higher-energy excited states. The intensity of the peak associated to L_b, is much smaller than the experimental one, confirming that our QD simulations underestimates the population of L_b. Moreover, it should be recalled that the intensity of the ESA peak predicted for the planar L_b minimum is much smaller than that computed for the real, non-planar one, and reported in Figure 2 of the main text and S7. Therefore, this discrepancy suggests that the non-planar minimum can be reached already before 100 fs.

c - 2. Energy barriers separating the different minima on the L_a PES.

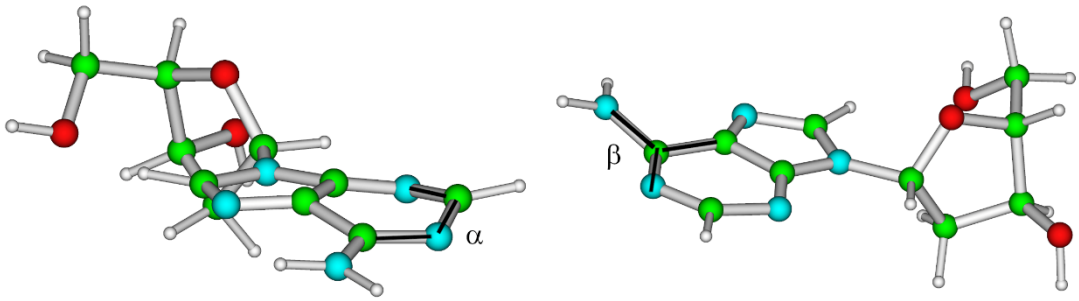

Figure S20 *Schematic description of the α and β dihedral angles (highlighted with a bold black line) used to characterize the energy barrier separating the different minima.*

We have explored the PES of dA in order to get information on the height of the energy barrier existing between the different minima on L_a, by performing geometry optimizations for different values of the C2N3N1C6 (α) and N10C6N1C5 (β) dihedral (Fig. S19), *i.e.* those associated to the out of plane motion of C2 and C6 groups.

L_a-min-pla and L_a-min-C2 are separated by an extremely small energy barrier (with α= 160°), of only 0.02 eV. Then, a further decrease of the α value (increasing the distortion of the

ring planarity) leads to the crossing region with S_0, which more stable than L_a-min-pla and L_a-min-C2. The energy barrier (with α~130°) associated with this process is also very small, *i.e.* ~0.02 eV from L_a-min-C2, in line with the ultrafast sub-ps decay of the excited state population. While exploring the crossing region with S_0, we located a fourth minimum, twisted at C2 (min-C2-tw, Fig. S3), which is more stable than all the other excited state minima and is located quite close to S_0, with an energy gap of 0.5 eV. However, due to its proximity to S0, it is not easy to ascertain the physical relevance of min-C2-tw, which could be a computational artefact. Indeed, it disappears when using a smaller basis set or another density functional. We stress that this minimum lies on the excited electronic state and not on the ground state, as those identified by Suzuki and coll. for pyrimidines.[29, 30] On the other hand, its presence its presence hints that part of the excited-state wave packet could be trapped near the crossing region.

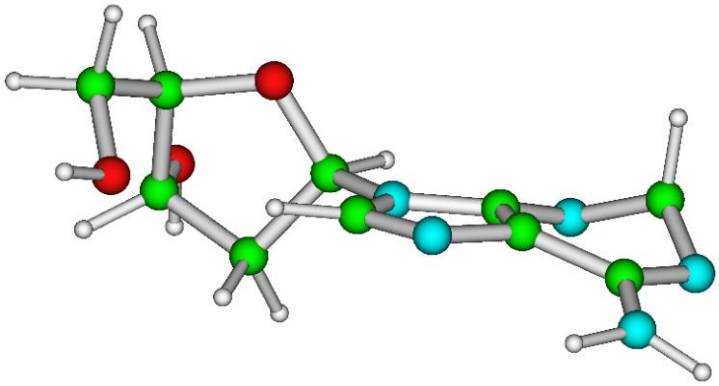

Figure S21*. Schematic description of the twisted minimum located for dA in the proximity of the crossing region with S0; PCM/TD-ωB97X-D/6-311+G(d,p) calculations.*

For what concerns the C6 path, the energy barrier separating L_a-min-pla and L_a-min-C6 is small, ~0.04 eV for β=150°. We also verified if a further decrease of β can lead to a crossing region with S_0. On the other hand, in this case, partial geometry optimizations along β were unsuccessful, with the system preferring to distort the ring along the N1C2N3 part, *i.e.* following the C2 path. As stated also in the main text, according to our calculations, and in agreement with the majority of the computational studies,[31-33] the C6 deactivation path is thus not expected to play a significant role.

References

(1) Petropoulos, V.; Martinez-Fernandez, L.; Uboldi, L.; Maiuri, M.; Cerullo, G.; Balanikas, E.; Markovitsi, D. Ultrafast dynamics of the UV-induced electronic relaxation in DNA guanine-thymine dinucleotides: from the Franck-Condon states to the minima of the potential energy surfaces. *Phys. Chem. Chem. Phys.* **2025**, *27*, 14936 - 14947. DOI: 10.1039/D5CP00788G.

(2) Borrego-Varillas, R.; Ganzer, L.; Cerullo, G.; Manzoni, C. Ultraviolet Transient Absorption Spectrometer with Sub-20-fs Time Resolution. *Appl. Sci.* **2018**, *8* (6), 989.

(3) Borrego-Varillas, R.; Oriana, A.; Branchi, F.; De Silvestri, S.; Cerullo, G.; Manzoni, C. Optimized ancillae generation for ultra-broadband two-dimensional spectral-shearing interferometry. *J. Opt. Soc. Am. B* **2015**, *32* (9), 1851-1855. DOI: 10.1364/josab.32.001851.

(4) Petropoulos, V.; Martinez-Fernandez, L.; Uboldi, L.; Maiuri, M.; Cerullo, G.; Balanikas, E.; Markovitsi, D. Real-time observation of sub-100-fs charge and energy transfer processes in DNA dinucleotides. *Chem. Sci.* **2024**, *15* (30), 12098-12107. DOI: 10.1039/d4sc02514h.

(5) Petropoulos, V.; Martinez-Fernandez, L.; Uboldi, L.; Maiuri, M.; Cerullo, G.; Balanikas, E.; Markovitsi, D. Factors Affecting the Population of Excited Charge Transfer States in Adenine/Guanine Dinucleotides: A Joint Computational and Transient Absorption Study. *Biomolecules* **2024**, *14* (12), 1548. DOI: 10.3390/biom14121548.

(6) Chai, J. D.; Head-Gordon, M. Long-range corrected hybrid density functionals with damped atom-atom dispersion corrections. *Phys. Chem. Chem. Phys.* **2008**, *10* (44), 6615-6620. DOI: 10.1039/b810189b.

(7) Tomasi, J.; Mennucci, B.; Cammi, R. Quantum mechanical continuum solvation models. *Chem. Rev.* **2005**, *105* (8), 2999-3093. DOI: 10.1021/cr9904009.

(8) Martinez-Fernandez, L.; Santoro, F.; Improta, R. Nucleic Acids as a Playground for the Computational Study of the Photophysics and Photochemistry of Multichromophore Assemblies. *Acc. Chem. Res.* **2022**, *55* (15), 2077-2087. DOI: 10.1021/acs.accounts.2c00256.

(9) *Gaussian 16 Rev. C.01*; Wallingford, CT, 2016. (accessed.

(10) Cerezo, J.; Santoro, F. FCclasses3: Vibrationally-resolved spectra simulated at the edge of the harmonic approximation. *J. Comput. Chem.* **2023**, *44* (4), 626-643. DOI: 10.1002/jcc.27027.

(11) Lu, T.; Chen, F. W. Multiwfn: A multifunctional wavefunction analyzer. *J. Comp. Chem.* **2012**, *33* (5), 580-592. DOI: 10.1002/jcc.22885.

(12) Green, J. A.; Yaghoubi Jouybari, M.; Asha, H.; Santoro, F.; Improta, R. Fragment Diabatization Linear Vibronic Coupling Model for Quantum Dynamics of Multichromophoric

Systems: Population of the Charge-Transfer State in the Photoexcited Guanine–Cytosine Pair. *J. Chem. Theory Comput.* **2021**, *17* (8), 4660-4674. DOI: 10.1021/acs.jctc.1c00416.

(13) Santoro, F.; Green, J. A. *Overdia 01, a Fortran 90 code for parametrization of model Hamiltonians based on a maximum-overlap diabatisation*. Concilio Nazionale de la Richerche, 2022. http://www.iccom.cnr.it/en/overdia-en/ (accessed 2026 11 March 2026).

(14) Beck, M. H.; Jäckle, A.; Worth, G. A.; Meyer, H. D. The multiconfiguration time-dependent Hartree (MCTDH) method: a highly efficient algorithm for propagating wavepackets. *Phys. Rep.* **2000**, *324* (1), 1-105. DOI: https://doi.org/10.1016/S0370-1573(99)00047-2.

(15) Meyer, H. D.; Manthe, U.; Cederbaum, L. S. The multi-configurational time-dependent Hartree approach. *Chem. Phys. Lett.* **1990**, *165* (1), 73-78. DOI: https://doi.org/10.1016/0009-2614(90)87014-I.

(16) Manthea, U. The multi-configurational time-dependent Hartree approach revisited. *J. Chem. Phys.* **2015**, *142* (24), 1-15. DOI: 10.1063/1.4922889 (acccessed 2026-03-27).Academic Search Ultimate.

(17) Wang, H. Multilayer Multiconfiguration Time-Dependent Hartree Theory. *J. Phys. Chem. A* **2015**, *119* (29), 7951-7965. DOI: 10.1021/acs.jpca.5b03256.

(18) Beck, M. H.; Jäckle, A.; Worth, G. A.; Meyer, H. D. The multiconfiguration time-dependent Hartree (MCTDH) method: a highly efficient algorithm for propagating wavepackets. *Physics Reports* **2000**, *324* (1), 1-105. DOI: https://doi.org/10.1016/S0370-1573(99)00047-2.

(19) Worth, G. A. Quantics: A general purpose package for Quantum molecular dynamics simulations. *Comput. Phys. Commun.* **2020**, *248*, 107040. DOI: https://doi.org/10.1016/j.cpc.2019.107040.

(20) Segatta, F.; Aranda, D.; Aleotti, F.; Montorsi, F.; Mukamel, S.; Garavelli, M.; Santoro, F.; Nenov, A. Time-Resolved X-ray Absorption Spectroscopy: An MCTDH Quantum Dynamics Protocol. *J. Chem. Theory Comput.* **2024**, *20* (1), 307-322. DOI: 10.1021/acs.jctc.3c00953.

(21) Avagliano, D.; Bonfanti, M.; Nenov, A.; Garavelli, M. Automatized protocol and interface to simulate QM/MM time-resolved transient absorption at TD-DFT level with COBRAMM. *J. Comp. Chem.* **2022**, *43* (24), 1641-1655. DOI: 10.1002/jcc.26966 From EBSCOhost mdl.

(22) Segatta, F.; Ruiz, D. A.; Aleotti, F.; Yaghoubi, M.; Mukamel, S.; Garavelli, M.; Santoro, F.; Nenov, A. Nonlinear Molecular Electronic Spectroscopy via MCTDH Quantum Dynamics: From Exact to Approximate Expressions. *Journal of Chemical Theory and Computation* **2023**, *19* (7), 2075-2091. DOI: 10.1021/acs.jctc.2c01059.

(23) Conti, I.; Bonfanti, M.; Nenov, A.; Rivalta, I.; Garavelli, M. Photo-Active Biological Molecular Materials: From Photoinduced Dynamics to Transient Electronic Spectroscopies. In *QM/MM Studies of Light-responsive Biological Systems*, Andruniov, T., Olivucci, M. Eds.; Springer Nature, 2020; pp 77–142.

(24) Picchiotti, A.; Nenov, A.; Giussani, A.; Prokhorenko, V. I.; Miller, R. J. D.; Mukamel, S.; Garavelli, M. Pyrene, a Test Case for Deep-Ultraviolet Molecular Photophysics. *J. Phy. Chem. Lett.* **2019**, *10* (12), 3481-3487. DOI: 10.1021/acs.jpclett.9b01325.

(25) Avila Ferrera, F. J.; Santoro, F. Comparison of vertical and adiabatic harmonic approaches for the calculation of the vibrational structure of electronic spectra. *Phys. Chem. Chem. Phys.* **2012**, *14*, 13549-13563.

(26) Fedotov, D. A.; Paul, A. C.; Koch, H.; Santoro, F.; Coriani, S.; Improta, R. Excited state absorption of DNA bases in the gas phase and in chloroform solution: a comparative quantum mechanical study. *Phys. Chem. Chem. Phys.* **2022**, *24* (8), 4987-5000. DOI: 10.1039/d1cp04340d.

(27) Nenov, A.; Giussani, A.; Segarra-Martí, J.; Jaiswal, V. K.; Rivalta, I.; Cerullo, G.; Mukamel, S.; Garavelli, M. Modeling the high-energy electronic state manifold of adenine: Calibration for nonlinear electronic spectroscopy. *J. Chem. Phys. Lett.* **2015**, *142* (21), 212443. DOI: 10.1063/1.4921016 (acccessed 6/29/2026).

(28) Assmann, M.; Köppel, H.; Matsika, S. Photoelectron Spectrum and Dynamics of the Uracil Cation. *J. Phys. Chem. A* **2015**, *119* (5), 866-875. DOI: 10.1021/jp512221x.

(29) Obara, Y.; Ghosh, S.; Humeniuk, A.; Kamibashira, S.; Adachi, S.; Suzuki, T. Formation of Ground-State Intermediate during Electronic Relaxation of Pyrimidine Nucleobases. *J. Am. Chem. Soc.* **2025**, *147* (18), 15077-15087. DOI: 10.1021/jacs.4c17415.

(30) Miura, Y.; Yamamoto, Y.; Karashima, S.; Orimo, N.; Hara, A.; Fukuoka, K.; Ishiyama, T.; Suzuki, T. Formation of Long-Lived Dark States during Electronic Relaxation of Pyrimidine Nucleobases Studied Using Extreme Ultraviolet Time-Resolved Photoelectron Spectroscopy. *J. Am. Chem. Soc.* **2023**, *145* (6). DOI: 10.1021/jacs.2c09803.

(31) Improta, R.; Santoro, F.; Blancafort, L. Quantum Mechanical Studies on the Photophysics and the Photochemistry of Nucleic Acids and Nucleobases. *Chem. Rev.* **2016**, *116* (6), 3540-3593. DOI: 10.1021/acs.chemrev.5b00444.

(32) Mansour, R.; Toldo, J. M.; Barbatti, M. Role of the Hydrogen Bond on the Internal Conversion of Photoexcited Adenosine. *J. Phys. Chem. Lett.* **2022**, *13* (26), 6194-6199. DOI: 10.1021/acs.jpclett.2c01554.

(33) Cuéllar-Zuquin, J.; Pepino, A. J.; Galván, I.; Rivalta, I.; Aquilante, F.; Garavelli, M.; Lindh, R.; Segarra-Martí, J. Characterizing Conical Intersections in DNA/RNA Nucleobases with Multiconfigurational Wave Functions of Varying Active Space Size. *J. Chem. Theory Comput.* **2023**, *19* (22), 8258-8272. DOI: 10.1021/acs.jctc.3c00577.